crystals

MDPI

Article

Design, Synthesis, and Biological Activity Evaluation of New Donepezil-Like Compounds Bearing Thiazole Ring for the Treatment of Alzheimer's Disease

Begüm Nurpelin Sağlık [1,2], Serkan Levent [1,2,*], Derya Osmaniye [1,2], Ulviye Acar Çevik [1,2], Betül Kaya Çavuşoğlu [3], Yusuf Özkay [1,2], Ali Savaş Koparal [4] and Zafer Asım Kaplancıklı [1]

1 Department of Pharmaceutical Chemistry, Faculty of Pharmacy, Anadolu University, 26470 Eskişehir, Turkey; bnsaglik@anadolu.edu.tr (B.N.S.); dosmaniye@anadolu.edu.tr (D.O.); uacar@anadolu.edu.tr (U.A.Ç.); yozkay@anadolu.edu.tr (Y.Ö.); zakaplan@anadolu.edu.tr (Z.A.K.)
2 Doping and Narcotic Compounds Analysis Laboratory, Faculty of Pharmacy, Anadolu University, 26470 Eskişehir, Turkey
3 Department of Pharmaceutical Chemistry, Faculty of Pharmacy, Zonguldak Bülent Ecevit University, 67600 Zonguldak, Turkey; betul.kcavusoglu@beun.edu.tr
4 Open Education Faculty, Anadolu University, 26470 Eskişehir, Turkey; askopara@anadolu.edu.tr
* Correspondence: serkanlevent@anadolu.edu.tr; Tel.: +90-222-335-0580/3778

Received: 25 June 2020; Accepted: 21 July 2020; Published: 23 July 2020

Abstract: Alzheimer's disease (AD) is a progressive and neurodegenerative disease that is primarily seen in the elderly population and is clinically characterized by memory and cognitive impairment. The importance of the disease has increased as a result of etiology of the disease having not yet been determined, an increase in patient population over the years, absence of radical treatment, high cost of treatment and care, and significant reduction in the quality of life of the patients, which have led researchers to direct more attention to this field. In a recent study, new indan-thiazolylhydrazone derivatives were designed and synthesized based on the chemical structure of the donepezil molecule, which is the most preferred and has the most appropriate response in the treatment of AD. The structures of the compounds were determined by ^{1}H-NMR and ^{13}C-NMR, and mass spectroscopic methods. Inhibition studies on the cholinesterase (ChE) enzymes and beta amyloid plaque inhibition test of the compounds were performed. Among the synthesized derivatives, compounds **2a**, **2e**, **2i**, and **2l** showed potent inhibitory activity on the AChE enzyme. Compound **2e** was found to be the most active agent, with an IC_{50} value of 0.026 μM. The mechanism of AChE inhibition by compound **2e** was studied using the Lineweaver-Burk plot, and the nature of inhibition was also determined to be mix-typed. Molecular docking studies were also carried out for compound **2e**, which was found as the most potent agent within the AChE enzyme active site. Moreover, compounds **2a**, **2e**, **2i**, and **2l** displayed the ability to prevent beta amyloid plaque aggregation at varying rates. In addition, ADME (Absorption, Distribution, Metabolism, Elimination) parameters were evaluated for all synthesized compounds using the *QikProp 4.8* software (Schrödinger Inc., NY, USA).

Keywords: Alzheimer's disease; anticholinesterase enzyme activity; beta amyloid plaque inhibition; donepezil; molecular docking; thiazolylhydrazone

1. Introduction

The elderly population is increasing worldwide. Due to this increase, the possibility of occurrence of dementia or mental diseases will rise as well. The main cause of dementia in the elderly is Alzheimer's disease (AD) [1]. AD is a neurodegenerative disease that is manifested by the gradual degradation of the cognitive, memory, and executive functions of the central nervous system (CNS). The lower

levels of acetylcholine (ACh) in patients with AD are associated with increased acetylcholinesterase (AChE) enzyme activity, which is known as the cholinergic hypothesis. Another important hypothesis for AD is known as the amyloid hypothesis, which comprises the formation and aggregation of the β-amyloid peptide (Aβ) caused by the hydrolysis of the amyloid precursor protein (APP) by β-secretase 1 (BACE-1). Drugs approved by the United States Food and Drug Administration for the clinical treatment of AD (such as donepezil, tacrine, etc.), particularly designed to inhibit the production of ACh, have a palliative effect [2].

In the brains of patients with AD, dramatically decreasing levels of ACh and butyrylcholine (BCh), which act as neuromediators, have been detected. The inhibition of the enzymes AChE and BChE, which hydrolyze ACh and BCh, has thus become an option for the treatment of AD. Therefore, research on the inhibition of these enzymes involved in the pathogenesis of AD is frequently conducted by many research groups. The observation of ACh reduction in AD patients, due to the loss of cholinergic neurons, establishes a strategy for the treatment [3]. Remarkably, the new information proposes that the decrease in cholinergic action and the accretion of β-amyloid plaques are related to each other. This relationship indicates that AChE increases the deposition of β-amyloid plaques, which in turn increases the expression of AChE. Significantly, brain levels of alternative enzymes that hydrolyse ACh, BChE, have shown progressive and significant increases in AD [4].

Among the numerous compounds developed as AChE inhibitors, donepezil is the most potent molecule since it provides a comparatively positive response in the treatment of AD. Additionally, nonhepatotoxicity, blood-brain barrier (BBB) permeability, a single daily dose, and the least side effects provide advantages for donepezil when compared to other AChE inhibitors [5]. Therefore, donepezil analogs have been studied more broadly [6–8].

The catalytic binding site (CAS) and peripheral anionic binding site (PAS) form the structure of AChE active site. The CAS specifically includes the Ser-His-Glu catalytic trio. A deep and hydrophobic gorge is composed by the PAS. Dual binding inhibitors bind to both sites, which is done by assembling a heterocyclic ring to benzylamine or a tacrine moiety through a linker of suitable length. The heterocyclic ring interacts with the PAS, while the other moiety binds to the CAS [9,10]. According to the molecular docking studies, donepezil also has the dual-binding mode of action. It was found that the presence of benzylamine contributes its inhibitory action by interacting with the CAS, while the indane moiety of the molecule, as a hydrophobic aromatic part, binds to the PAS [11–14].

This study aimed to find new ChE inhibitors. The 6-methoxyindane structure was fused to a thiazolylhydrazone moiety to design and synthesize new donepezil analogues. For the inhibition of AChE through binding to the PAS, the 6-methoxyindane ring was used, due to its aromatic character, while a thiazolylhydrazone moiety, such as a benzylamine structure, was used for its potential interaction with the CAS (Figure 1). Accordingly, in the present study, the design, synthesis, biological activity evaluation, and molecular modeling studies of a new series of donepezil-like compounds was presented as potent agents for the treatment of AD.

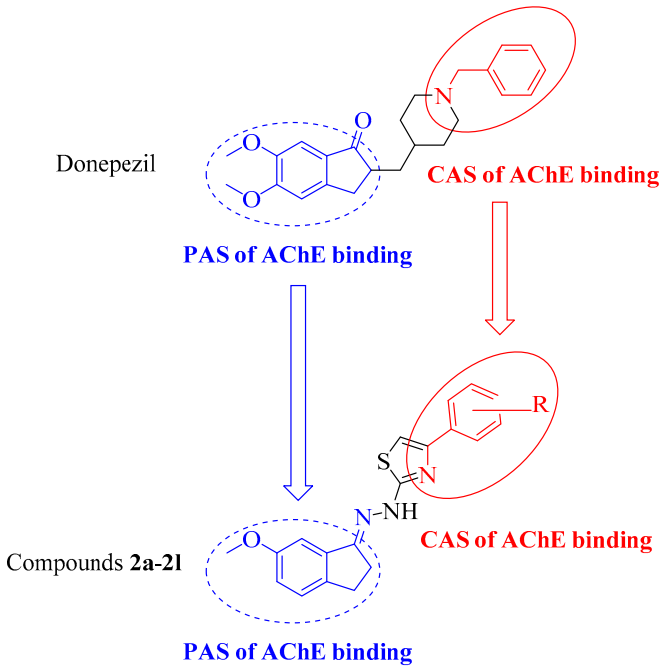

Figure 1. Design of the target compounds **2a–2l** from donepezil.

2. Results and Discussion

2.1. Chemistry

The compounds **2a–2l** were synthesized as outlined in Scheme 1. First, 2-(6-methoxy-2,3-dihydro-1*H*-inden-1-ylidene)hydrazine-1-carbothioamide (**1**) was synthesized by a reaction of 6-methoxy-indan-1-one and thiosemicarbazide, which was performed in ethanol with a catalytic amount of CH_3COOH. Finally, target compounds (**2a–2l**) were prepared through the ring closure reaction using the obtained 2-(6-methoxy-2,3-dihydro-1*H*-inden-1-ylidene)hydrazine-1-carbothioamide (**1**) and an appropriate 2-bromoacetophenone derivative. The substituents of the final compounds are presented in Table 1.

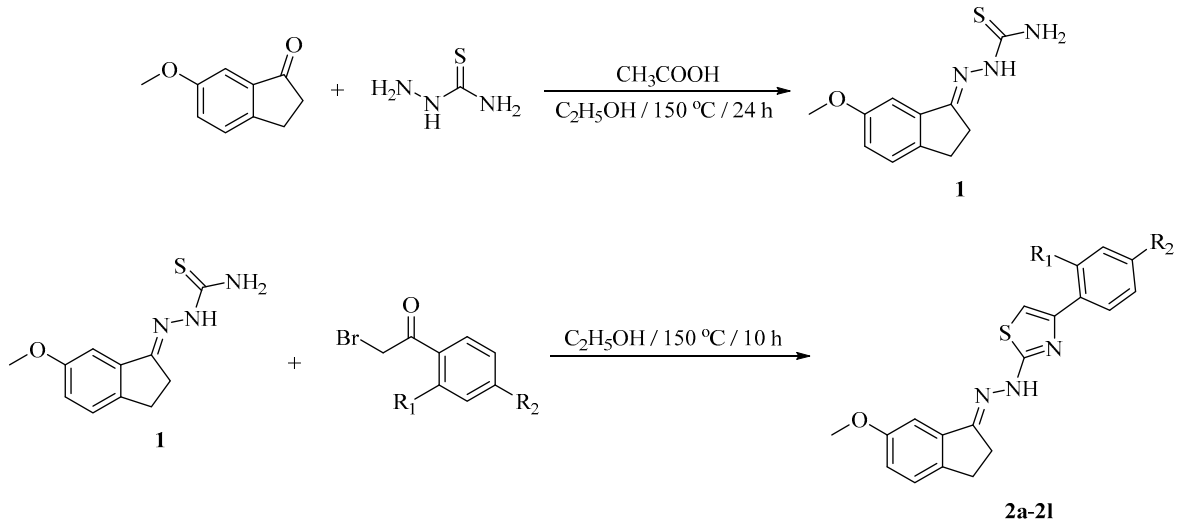

Scheme 1. Synthesis of compounds **2a–2l.**

Table 1. Substituents of the final compounds.

Compounds	R_1	R_2
2a	–H	–H
2b	–H	$–CH_3$
2c	–H	$–OCH_3$
2d	–H	–CN
2e	–H	$–NO_2$
2f	–H	–F
2g	–H	–CI
2h	–H	–Br
2i	$–CH_3$	$–CH_3$
2j	$–OCH_3$	$–OCH_3$
2k	–F	–F
2l	–CI	–CI

2.2. Cholinesterase Enzymes Inhibition Assay

All the obtained 6-methoxyindane-thiazolylhydrazone derivatives were investigated for their inhibitory activity against the cholinesterase enzymes using the previously described in vitro modified Ellman's spectrophotometric method [7,15–22].

The assay was performed in two steps. The first step was carried out using all of the synthesized compounds and reference agents, namely donepezil and tacrine, at concentrations of 1000 and 100 μM. The enzyme activity results of the first step are presented in Table 2. Next, the selected compounds that displayed more than 50% inhibitory activity at concentrations of 1000 and 100 μM were further tested, along with the reference agents, at concentrations of 10 to 0.001 μM. The IC_{50} values of the test compounds and reference agents are presented in Table S1 (Supplementary Material).

Table 2. Inhibition (%) of the synthesized compounds, donepezil, and tacrine against acetylcholinesterase (AChE) and butyrylcholine (BChE) enzymes.

Compounds	AChE % Inhibition		AChE IC_{50} (μM)	BChE % Inhibition	
	1000 μM	100 μM		1000 μM	100 μM
2a	90.28 ± 1.95	84.36 ± 1.05	0.118 ± 0.004	48.12 ± 0.85	31.45 ± 0.62
2b	85.65 ± 1.20	47.38 ± 0.95	-	35.20 ± 0.91	24.86 ± 0.59
2c	88.34 ± 1.00	46.26 ± 0.97	-	34.45 ± 0.97	28.13 ± 0.61
2d	80.48 ± 1.34	48.71 ± 0.85	-	30.50 ± 0.85	23.47 ± 0.52
2e	98.56 ± 1.85	94.14 ± 1.69	0.026 ± 0.001	46.25 ± 0.90	32.75 ± 0.73
2f	75.16 ± 1.26	43.30 ± 0.90	-	35.61 ± 0.72	28.45 ± 0.63
2g	73.66 ± 0.95	41.97 ± 0.97	-	29.15 ± 0.76	21.74 ± 0.57
2h	78.96 ± 1.46	46.38 ± 0.89	-	32.59 ± 0.84	27.21 ± 0.61
2i	92.45 ± 1.60	86.49 ± 1.24	0.070 ± 0.003	45.95 ± 0.92	30.65 ± 0.80
2j	82.50 ± 1.51	48.20 ± 0.89	-	30.61 ± 0.71	24.87 ± 0.69
2k	77.36 ± 1.64	47.21 ± 0.97	-	28.30 ± 0.63	21.47 ± 0.71
2l	91.28 ± 1.85	86.46 ± 1.30	0.061 ± 0.002	49.32 ± 0.97	33.54 ± 0.87
Donepezil	99.25 ± 2.10	97.42 ± 1.89	0.021 ± 0.001	-	-
Tacrine	-	-	-	98.25 ± 1.89	95.46 ± 1.34

According to the enzyme inhibition results, none of the synthesized compounds showed significant activity against the BChE enzyme. All compounds displayed selective inhibition to AChE. At a concentration of 1000 μM, all the compounds showed more than 50% inhibitory activity.

Compounds **2a**, **2e**, **2i**, and **2l** passed the second step of the enzyme activity assay and their IC_{50} values were calculated by performing an enzyme inhibition study at concentrations of 10 to 0.001 μM. The IC_{50} values of compounds **2a**, **2e**, **2i**, and **2l** were calculated as 0.118, 0.026, 0.070, and 0.061 μM, respectively. Among these derivatives, compound **2e** was found to be the most active agent in the

series, with an IC_{50} value of 0.026 μM. It was seen that compound **2e** exhibited an inhibition profile similar to the reference drug, donepezil (IC_{50} value = 0.021 μM).

Among the actively detected compounds, **2i** and **2l** carried dimethyl and dichloro substituents, respectively, at the *ortho*- and *para*- positions of the phenyl ring. According to the enzyme inhibition results, it was thought that the substituents, especially at the *ortho*- position of the phenyl ring, positively contributed to the enzyme inhibition capacity. Moreover, compound **2e**, which was determined to be the most potent derivative, had a nitro substituent at the *para*- position of the phenyl ring. Due to the nitro substituent in this compound, it can be suggested that the electron withdrawing group made a very important contribution to enhancing inhibition potency against the AChE.

2.3. Kinetic Studies of Enzyme Inhibition

Enzyme kinetics studies were performed to determine the mechanism of the AChE inhibition using a procedure similar to that of the cholinesterase enzymes inhibition assay. Compound **2e**, which was found to be the most potent agent, was included in these studies. In order to estimate the type of inhibition of this compound, linear Lineweaver-Burk graphs were used. Substrate velocity curves in the absence and presence of compound **2e** were recorded. This compound was prepared at concentrations of $IC_{50}/2$, IC_{50}, and $2 \times IC_{50}$ for the enzyme kinetic studies. In each case, the initial velocity measurements were obtained at different substrate (ATC) concentrations, ranging from 600 to 18.75 μM. The secondary plots of the slope (K_m/V_{max}) versus varying concentrations (0, $IC_{50}/2$, IC_{50}, and $2 \times IC_{50}$) were created to calculate the K_i (intercept on the x-axis) value of this compound. The graphical analyses of the steady-state inhibition data for compound **2e** are shown in Figure 2.

According to the Lineweaver-Burk plots, a graph with lines that do not intersect at the x-axis or the y-axis is formed for a mixed-type inhibition. Therefore, as shown in Figure 2, compound **2e** was reversible and had mixed-type inhibitors with similar inhibition features to the substrates. K_i values for compound **2e** were calculated as 0.022 μM for inhibition of the AChE.

Irreversible enzymatic inhibition involves covalent interactions between the substrate and the enzyme. In contrast, there are non-covalent interactions, such as hydrophobic interactions, ionic bonds, and hydrogen bonds, involved in reversible inhibition. In this type of inhibition, inhibitors bind to the enzymes without forming any chemical bonds; thus, the enzyme-inhibitor complex could be separated quickly, because non-covalent interactions can form rapidly and break easily. Furthermore, reversible inhibitors have a lower risk of side effects than irreversible inhibitors, owing to their non-covalent binding ability. Consequently, compound **2e**, whose inhibition type was determined to be reversible and mix-typed, has a pharmaceutical importance for being an inhibitor candidate of the AChE enzyme.

2.4. Inhibition of Beta Amyloid 1–42 (Aβ42) Aggregation

The accumulation of amyloid plaques that can be found in the brains of patients suffering from AD is another important reason as well as decreasing cholinergic transmission. Plaques are mainly composed of beta amyloid (Aβ) peptides. Recent studies have shown that two beta amyloid peptides (Aβ (1–40) and Aβ (1–42)) exist in brain tissues, cerebrospinal fluid (CSF), and plasma in patients suffering from AD. Therefore, screening of Aβ42 ligands that can prevent aggregation is critical for the development of potential therapeutic treatments. Hence, in this study, for the selected compounds, **2a**, **2e**, **2i**, and **2l**, which displayed potent inhibitory activity against the AChE enzyme, the inhibition of beta amyloid 1–42 (Aβ42) aggregation was evaluated using the beta amyloid 1–42 (Aβ42) ligand screening assay kit (BioVision, Milpitas, CA, USA). This assay kit is based on the fluorometric method and the assay procedure was applied according to the instructions of this kit. In the presence of an Aβ42 ligand, this reaction is impeded/abolished, resulting in a decrease or total loss of fluorescence. The percentage of inhibition of beta amyloid 1–42 (Aβ42) peptides aggregation are given in Figure 3 for compounds **2a**, **2e**, **2i**, and **2l**. These compounds were tested at concentrations of 100 and 10 μM, and the Aβ42 inhibitor included in the kit was used as the standard. All of the test compound concentrations were applied in quadruplicate in the plates.

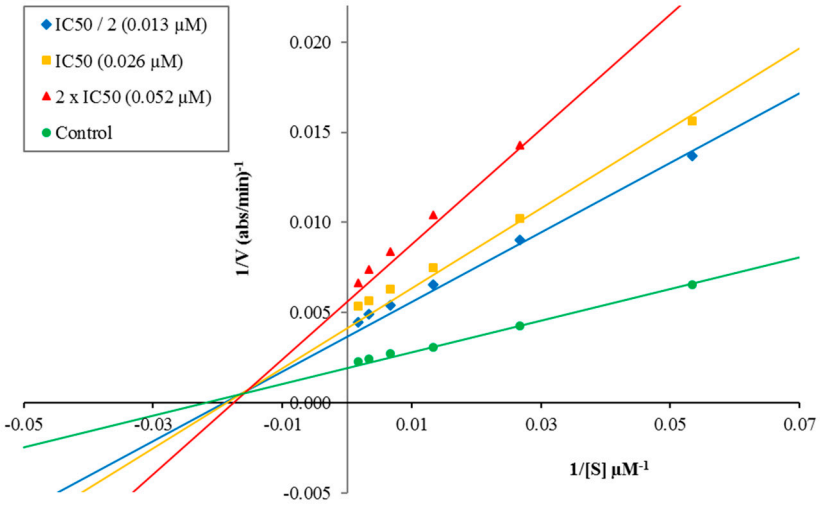

(**A**)

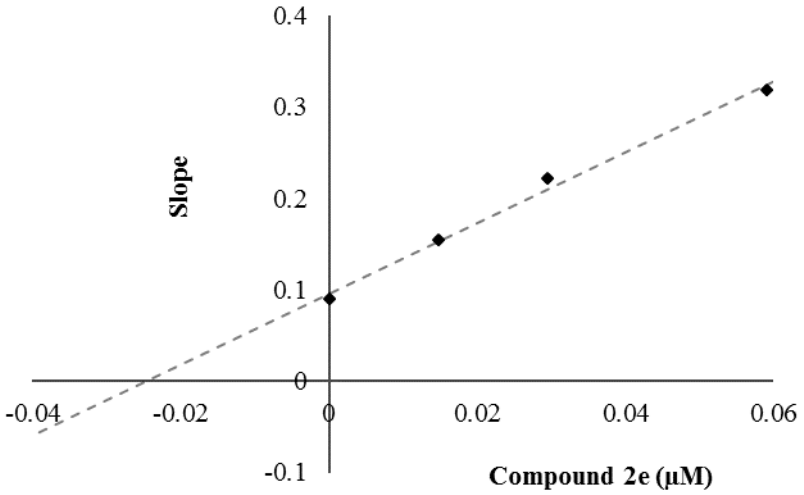

(**B**)

Figure 2. (**A**) Lineweaver-Burk plots for the inhibition of AChE by compound **2e**. [S], substrate concentration (µM); V, reaction velocity (1/V (abs/min)$^{-1}$). Inhibitor concentrations are shown at the left. (**B**) Secondary plot for the calculation of the steady-state inhibition constant (K_i) of compound **2e**. K_i was calculated as 0.022 µM.

According to Figure 3, compounds **2a**, **2e**, **2i**, and **2l** showed more than 50% inhibition at a concentration of 100 µM. The percentage of inhibition of compounds **2a**, **2e**, **2i**, and **2l** at this concentration was as follows: 71.87%, 87.36%, 77.16%, and 82.51%, respectively. At a concentration of 10 µM, only compound **2e** displayed more than 50% inhibition, namely 73.45%. These findings indicated that the related compounds had the ability to prevent beta amyloid plaque aggregation at varying rates, in addition to their AChE enzyme inhibitory potential.

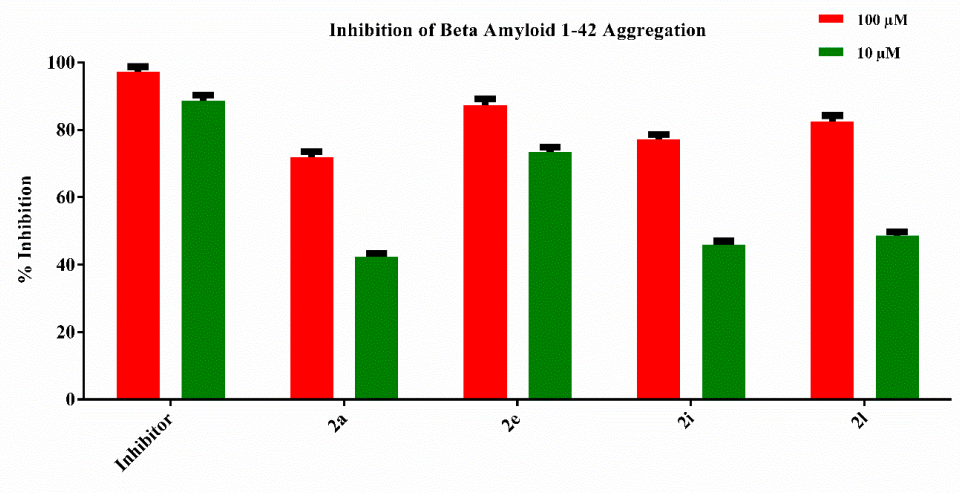

Figure 3. Beta amyloid plaque inhibition (%) of compounds **2a**, **2e**, **2i,** and **2l**.

2.5. Prediction of ADME Parameters and BBB Permeability

In this study, the ADME (Absorption, Distribution, Metabolism, Elimination) parameters of the synthesized compounds (**2a**–**2l**) were evaluated using the *QikProp 4.8* software (Schrödinger Inc., NY, USA) [23].

Lipinski and Jorgensen defined physicochemical ranges for active compounds that are likely to be oral drugs. Based on the relationship between pharmacokinetic and physicochemical parameters, Lipinski's rule of five and Jorgensen's rule of three are used to determine the structural properties sought in a candidate compound that may be a drug [24,25]. Moreover, these rules are known as drug-like testing [26]. The calculated ADME parameters, including molecular weight (MW), number of rotatable bonds (RB), dipole moment (DM), molecular volume (MV), number of hydrogen donors (DHB), number of hydrogen acceptors (AHB), polar surface area (PSA), octanol/water partition coefficient (log P), aqueous solubility (log S), apparent Caco-2 cell permeability (PCaco), number of likely primer metabolic reactions (PM), percent of human oral absorption (%HOA), and the violations of the rules of three (VRT) and five (VRF) are presented in Table 3. It can be seen from this table that all of the parameters were within the reference ranges. In keeping with Jorgensen's rule of three and Lipinski's rule of five, the obtained compounds (**2a**–**2l**) were in accordance with the set parameters, as they did not cause more than one violation. Considering the results of the ADME parameter studies, the synthesized compounds had pharmacokinetic profiles that may be appropriate for clinical use.

Drugs that specifically target the CNS must first cross the BBB (blood brain barrier). Although the BBB is protective in nature, the use of drug candidates that affect the CNS in the clinical setting is unlikely if such drug molecules cannot penetrate it. For this reason, this feature must be explored earlier in the drug discovery process. Accordingly, it is of great importance to predict the BBB permeability of new compounds [27]. Therefore, the BBB permeability of the obtained compounds (**2a**–**2l**) was also evaluated using the *QikProp 4.8* software [23]. Brain/blood partition coefficient (logBB) and apparent MDCK cell permeability (PMDCK) were calculated for this purpose. In keeping with the software estimates, the PMDCK values of < 25 and > 500 nm/s were determined as poor and great for non-active transport of the compounds. To evaluate the ability of a compound to pass through the BBB, logBB is another important parameter to consider with the recommended values between -3 and $+1.2$. The PMDCK and logBB values of the synthesized compounds are within the advised ranges as shown in Table 3. Therefore, it can be assumed that the synthesized compounds can exceed the BBB, which is very important for CNS-related drugs.

Considering the results of the ADME and BBB permeability studies, the synthesized compounds were determined to have pharmacokinetic profiles that may be appropriate for clinical use.

Table 3. Calculated ADME (Absorption, Distribution, Metabolism, Elimination) parameters of compounds **2a**–**2l**.

Comp.	MW	RB	DM	MV	DHB	AHB	PSA	logP	logS	PCaco	logBB	PMDCK	CNS	PM	%HOA	VRF	VRT
2a	335.42	4	3.332	1083.4	1	4.25	42.958	4.743	−5.854	5528.688	0.180	6206.560	1	4	100	0	1
2b	349.45	4	2.840	1142.4	1	4.25	42.958	5.048	−6.419	5528.688	0.173	6206.560	1	5	100	1	1
2c	360.43	5	9.732	1150.1	1	5.75	68.754	3.942	−6.827	1143.337	−0.664	1129.910	0	4	100	0	1
2d	365.45	5	3.596	1151.2	1	5	51.440	4.788	−5.983	5528.686	0.115	6206.559	1	5	100	0	1
2e	380.42	5	13.462	1165.8	1	5.25	91.625	4.049	−6.113	568.231	−1.004	530.683	2	5	100	0	1
2f	353.41	4	5.778	1099.6	1	4.25	42.963	4.979	−6.220	5528.423	0.293	10,000	1	4	100	0	1
2g	369.87	4	5.724	1127.6	1	4.25	42.961	5.238	−6.597	5528.522	0.350	10,000	1	4	100	1	1
2h	414.32	4	5.405	1136.5	1	4.25	42.961	5.315	−6.713	5528.586	0.363	10,000	1	4	100	1	1
2i	363.48	4	3.336	1167.2	1	4.25	38.069	5.240	−6.216	6852.418	0.288	7827.314	1	6	100	1	1
2j	395.48	6	2.543	1202.8	1	5.75	55.272	4.786	−5.508	5876.146	0.100	6629.222	1	6	100	0	0
2k	371.40	4	5.143	1108.3	1	4.25	41.521	5.129	−6.404	5803.010	0.383	10,000	1	4	100	1	1
2l	404.31	4	5.201	1140.4	1	4.25	39.548	5.444	−6.460	6255.627	0.496	10,000	2	4	100	1	1

MW: Molecular weight; **RB:** Number of rotatable bonds (recommended value: 0−15); **DM:** Computed dipole moment (recommended value: 1–12.5); **MV:** Total solvent-accessible volume (recommended value: 500–2000); **DHB:** Estimated number of hydrogen bond donors (recommended value: 0–6); **AHB:** Estimated number of hydrogen bond acceptors (recommended value: 2–20); **PSA:** Van der Waals surface area of polar nitrogen and oxygen atoms and carbonyl carbon atoms (recommended value: 7–200); **logP:** Predicted octanol/water partition coefficient (recommended value: −2–6.5); **logS:** Predicted aqueous solubility (recommended value: −6.5–0.5); **PCaco:** Predicted apparent Caco-2 cell permeability (recommended value: <25 poor, >500 great); **logBB:** Predicted brain/blood partition coefficient (recommended value: −3–1.2); **PMDCK:** Predicted apparent MDCK cell permeability (recommended value: <25 poor, >500 great); **CNS:** Predicted central nervous system activity on a −2 (inactive) to +2 (active) scale (recommended value: −2 (inactive), +2 (active)); **PM:** Number of likely metabolic reactions (recommended value: 1–8); **%HOA:** Predicted human oral absorption percent (recommended value: > 80% is high, <25% is poor); **VRF:** Number of violations of Lipinski's rule of five. The rules are: MW < 500, logP < 5, DHB ≤ 5, AHB ≤ 10, positive PSA value. **VRT:** Number of violations of Jorgensen's rule of three. The three rules are: logS > −5.7, PCaco > 22 nm/s, PM < 7.

2.6. Molecular Docking

As mentioned in the cholinesterase enzymes inhibition assay, compound **2e** was found to be the most active derivative in the series against the AChE enzyme. Hence, docking studies were carried out to evaluate its inhibition capability in silico. Obtaining more insight into the binding mode of compound **2e** and an evaluation of the effects of the structural modifications on the inhibitory activity against the AChE enzyme was made possible as a result of the docking studies. These studies were carried out using the X-ray crystal structure of *Homo sapiens* AChE (*h*AChE PDB ID:4EY7) [12] retrieved from the Protein Data Bank server (www.pdb.org). The reason for choosing this X-ray crystal structure was that it was human in origin, had a high resolution, and contained the donepezil molecule as the ligand. First, the docking procedure was confirmed by performing the protocol with donepezil. Next, compound **2e** was subjected to the same docking procedure. The rendered docking poses of the donepezil and compound **2e** are provided in Figures 4 and 5.

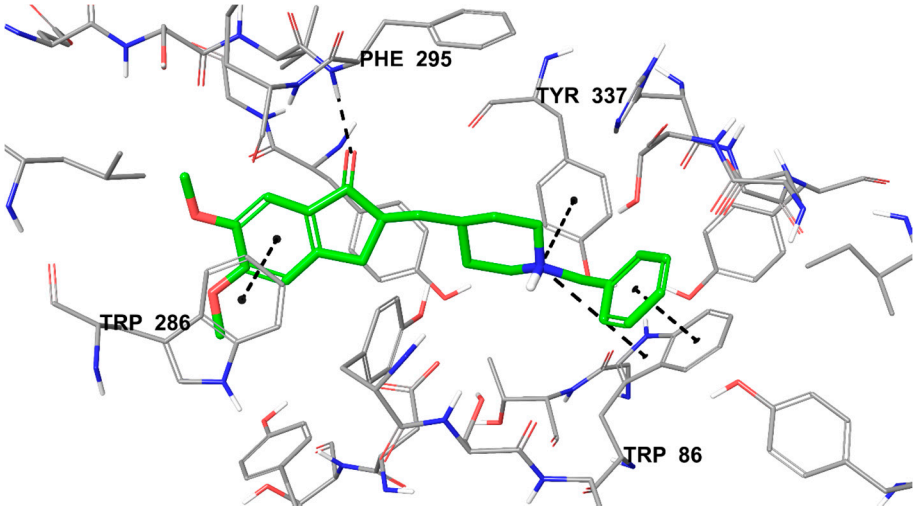

Figure 4. The three-dimensional interacting mode of donepezil in the active region of AChE. Donepezil, colored with green, and the important residues, colored with grey, in the active site of the enzyme are presented by the tube model (AChE PDB Code: 4EY7).

According to the X-ray crystallographic structure of AChE (PDB ID:4EY7), the enzyme active pocket consisted of two main binding sites, the CAS and PAS. The CAS contained Ser203, Glu334, His447, Trp86, Tyr130, Tyr133, Tyr337, and Phe338 amino acid residues; however, amino acids Tyr72, Asp74, Tyr124, Trp286, Phe295, and Tyr341 were located in the PAS [28–31]. Donepezil interacts with both the CAS and PAS. Therefore, it can be settled into the gorge concordantly as a result of its dual binding site (DBS) [32–34]. According to Figure 4, the benzyl moiety of donepezil has a π-π interaction with the indole of Trp86. Furthermore, the protonated nitrogen atom of piperidine forms cation-π interactions with the indole of Trp86 and the phenyl of Tyr337. Thus, the benzylpiperidine group of donepezil is strongly located in the CAS. The interactions of the 1-indanone ring are important for binding to the PAS. The 1-indanone constitutes a π-π interaction with the indole of Trp286. Moreover, there is a hydrogen bond formation between the carbonyl of the 1-indanone and the amine of Phe295. These identified interactions of donepezil were consistent with the data in the literature and the docking procedure was verified via these findings [12,35–37].

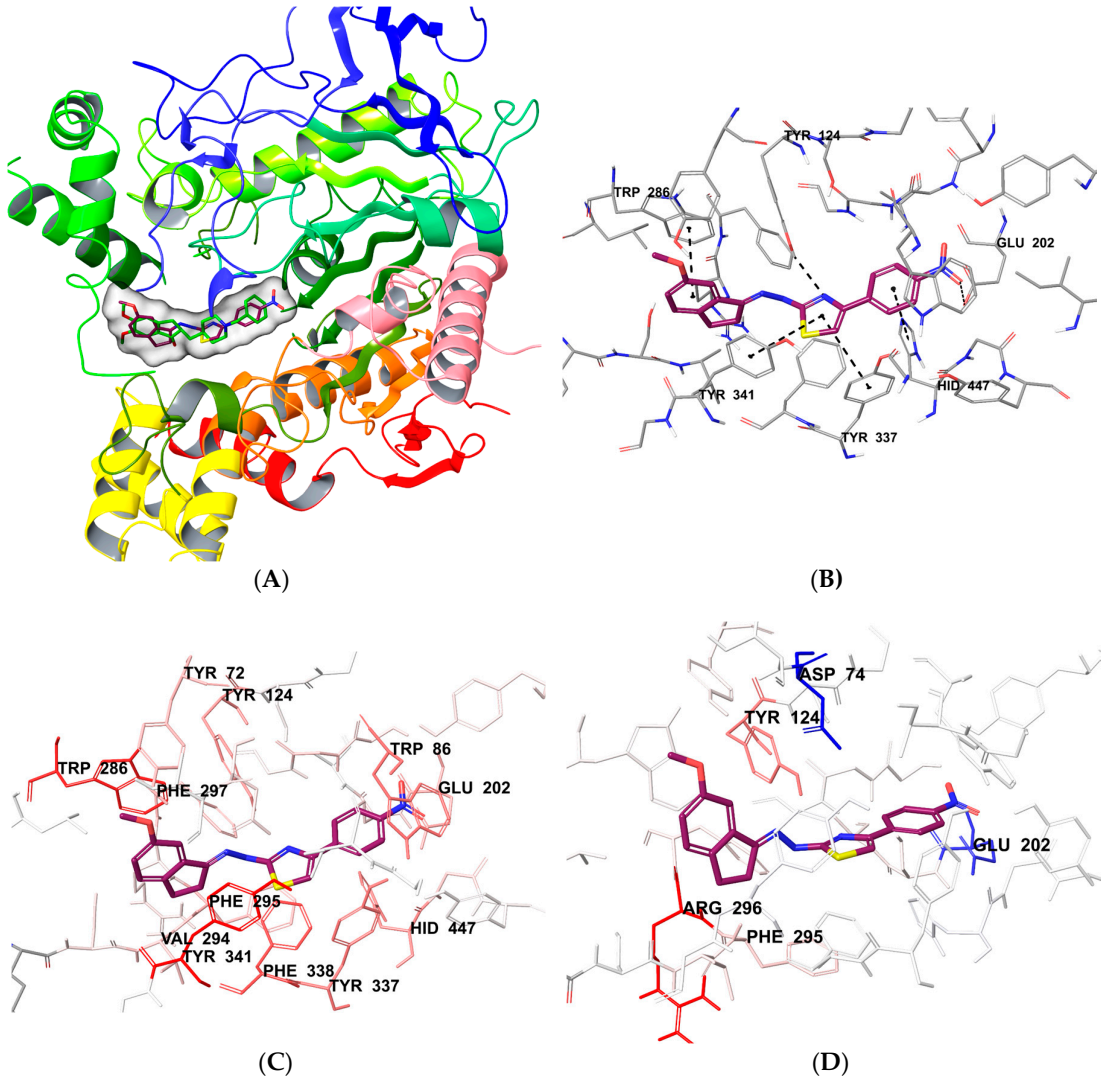

Figure 5. (**A**) The superimposition pose of compound **2e** and donepezil in the enzyme active site. Compound **2e** and donepezil are colored with maroon and green, respectively. (**B**) The three-dimensional interacting mode of compound **2e** in the active region of AChE. The inhibitor, colored with maroon, and the important residues, colored with grey, in the active site of the enzyme are presented by the tube model. (**C**) The Van der Waals interaction of compound **2e** with the active region of AChE. The active ligand has a lot of favorable Van der Waals interactions (red and pink). (**D**) The electrostatic interaction of compound **2e** with the active region of AChE. The residues are colored (blue, red, and pink) according to the distance from the ligand by a Per-Residue Interaction panel (AChE PDB Code: 4EY7).

Figure 5A presents the superimposition of donepezil and compound **2e** in the active region of the AChE. It was clear that compound **2e** bound to the active site of the AChE enzyme in a similar position as donepezil due to its dual binding sites. This compound mainly carries the lipophilic indan ring, 4-substituedphenyl-thiazole group, as a polar group, and a basic center. The docking poses indicated that lipophilic groups interacted with the PAS region, whereas the polar and basic groups bound to the CAS region.

The docking pose of compound **2e** (Figure 5B) revealed that the indan ring created a π-π interaction with the indole of Trp286. This interaction was the same as that with donepezil in relation to the PAS region. Moreover, it was seen that the thiazole ring in the middle of the structure was essential to attain strong binding. A hydrogen bond was observed between the nitrogen atom of the thiazole ring and the hydroxyl of Tyr124. This interaction highlighted the binding to the CAS region, as in the donepezil

via the benzylamine moiety. The thiazole ring established two π-π interactions with the phenyl rings of Tyr337 and Tyr341. Thus, it can be said that the thiazole ring interacted with both the CAS and PAS, owing to these interactions with the Tyr337 and Tyr341 amino acid residues. In addition, the phenyl ring near the thiazole ring had a π-π interaction with the imidazole of Hid447. This interaction was a proof of binding to the PAS. Moreover, the nitro substituent of the phenyl ring was important for polar interaction. The oxygen atom of the nitro formed a hydrogen bond with the hydroxyl of Glu202.

Structurally, the main difference between compound **2e** and the other derivatives was the nitro group at the *para*- position of the phenyl ring. In this context, the docking studies supported the enzyme inhibition results. It was thought that the interactions related to the nitro group at the *para*-position of the phenyl ring were important in terms of explaining its inhibitory activity against the AChE enzyme. It was seen that the presence of an electron withdrawing group, such as nitro, at this position was a positive contribution to the activity.

In order to analyze the contribution of the van der Waals and electrostatic interactions in binding to the enzyme active site, docking studies were performed using Glide (Schrödinger, NY, USA), according to the per-residue interaction panel. Figure 5C,D presents the van der Waals and electrostatic interactions of compound **2e**. As is shown, this compound had favorable van der Waals interactions with amino acids Tyr72, Trp86, Tyr124, Glu202, Trp286, Val294, Phe295, Phe297, Tyr337, Phe338, Tyr341, and Hid447, which are displayed in pink and red, as described in the Glide user manual [38]. Similarly, promising electrostatic contributions of compound **2e** were determined with amino acids Asp74, Tyr124, Glu202, Phe295, and Arg296.

3. Materials and Methods

3.1. Chemistry

All the chemicals used in the synthesis studies were obtained from Merck (Darmstadt, Germany) or Sigma-Aldrich (St. Louis, MO, USA). A MP90 digital melting point apparatus (Mettler Toledo, OH, USA) was used to determine the melting points of the resulting compounds and was presented uncorrected. A Bruker 300 and 75 MHz digital FT-NMR spectrometer (Billerica, MA, USA) in DMSO-d_6, respectively, was used to record the ^{1}H-NMR and ^{13}C-NMR spectra. In the NMR spectra, the splitting patterns were determined and recognized as follows: s: Singlet, d: Doublet, t: Triplet, dd: Double doublet, td: Triple doublet, brs: Bronsted singlet, and m: Multiplet. Coupling constants (*J*) were reported in units of Hertz (Hz). Mass spectra were recorded on a Shimadzu 8040 LC-MS-MS spectrophotometer (Kyoto, Japan). ^{1}H-NMR and ^{13}C-NMR spectra (Figures S1–S24) are available in the Supplementary Material file.

3.1.1. General Procedure for the Synthesis of the Compounds

Synthesis of 2-(6-methoxy-2,3-dihydro-1*H*-inden-1-ylidene)hydrazine-1-carbothioamide (**1**)

For synthesis of the 2-(6-methoxy-2,3-dihydro-1*H*-inden-1-ylidene)hydrazine-1-carbothioamide (**1**), 6-methoxy-indan-1-one (4.050 g, 0.025 mol) and thiosemicarbazide (2.275 g, 0.025 mol) were reacted in the presence of a catalytic quantity of acetic acid (CH_3COOH), and the obtained mixture was refluxed in EtOH (50 mL) for 24 h. The reaction mixture was cooled after the completion of the reaction. Finally, the precipitated product was filtered, washed with cold ethanol, dried, and recrystallized from methanol [39].

General Procedure for the Synthesis of Target Compounds (**2a**–**2l**)

For the synthesis of the target compounds (**2a**–**2l**), to a stirred solution of 2-(6-methoxy-2,3-dihydro-1*H*-inden-1-ylidene)hydrazine-1-carbothioamide (**1**) (0.353 g, 0.0015 mmol) in EtOH (20 mL), appropriate 2-bromo-1-(substituted phenyl)ethan-1-one derivatives (0.0015 mmol) were added, and

then refluxed for 10 h. The precipitated product was filtered, washed with cold ethanol, dried, and recrystallized from EtOH.

2-(2-(6-methoxy-2,3-dihydro-1H-inden-1-ylidene)hydrazineyl)-4-phenylthiazole (**2a**) Yield: 81%. M.P.: 230–232 °C. ^{1}H-NMR (300 MHz, DMSO-d_6): δ = 2.91 (2H, t, *J* = 5.8 Hz, –CH_2), 3.01 (2H, t, *J* = 5.9 Hz, –CH_2), 3.79 (3H, s, –OCH_3), 6.97 (1H, dd, *J* = 8.3 Hz, 2.5 Hz, indanimine H_4), 7.10 (1H, d, *J* = 2.4 Hz, indanimine H_2), 7.28 (1H, d, *J* = 8.6 Hz, indanimine H_5), 7.32–7.35 (2H, m, phenyl CH, thiazole CH), 7.43 (2H, t, *J* = 7.5 Hz, Phenyl CH), 7.85 (2H, d, *J* = 7.1 Hz, Phenyl CH), 11.10 (1H, brs, NH). ^{13}C-NMR (75 MHz, DMSO-d_6): δ = 27.8, 28.8, 55.8, 104.4, 118.4, 126.2, 127.0, 128.3, 128.8, 129.1, 134.2, 139.2, 140.9, 149.2, 157.9, 159.2, 169.7. ESI-MS (*m*/*z*): $[M + H]^+$: 336.

2-(2-(6-methoxy-2,3-dihydro-1H-inden-1-ylidene)hydrazineyl)-4-(4-methylphenyl)thiazole (**2b**) Yield: 83%. M.P.: 243–245 °C. ^{1}H-NMR (300 MHz, DMSO-d_6): δ = 2.32 (3H, s, –CH_3), 2.90 (2H, t, *J* = 6.3 Hz, –CH_2), 3.01 (2H, t, *J* = 6.2 Hz, –CH_2), 3.80 (3H, s, –OCH_3), 6.96 (1H, dd, *J* = 8.3 Hz, 2.5 Hz, indanimine H_4), 7.08 (1H, d, *J* = 2.4 Hz, indanimine H_2), 7.21–7.24 (3H, m, tolyl CH, thiazole CH), 7.28 (1H, d, *J* = 8.4 Hz, indanimine H_5), 7.76 (2H, d, *J* = 8.1 Hz, tolyl CH), 11.16 (1H, brs, NH). ^{13}C-NMR (75 MHz, DMSO-d_6): δ = 21.3, 27.8, 28.7, 55.8, 103.4, 104.2, 118.2, 126.0, 126.9, 129.7, 132.3, 134.8, 137.3, 139.4, 140.7, 156.9, 159.2, 169.7. ESI-MS (*m*/*z*): $[M + H]^+$: 350.

2-(2-(6-methoxy-2,3-dihydro-1H-inden-1-ylidene)hydrazineyl)-4-(4-methoxyphenyl)thiazole (**2c**) Yield: 80%. M.P.: 236–238 °C. ^{1}H-NMR (300 MHz, DMSO-d_6): δ = 2.91 (2H, t, *J* = 7.2 Hz, –CH_2), 3.00 (2H, t, *J* = 6.9 Hz, –CH_2), 3.79 (3H, s, –OCH_3), 3.80 (3H, s, –OCH_3), 6.96–7.00 (3H, m, methoxyphenyl CH, indanimine H_4), 7.10 (1H, d, *J* = 2.3 Hz, indanimine H_2), 7.17 (1H, s, thiazole CH), 7.28 (1H, d, *J* = 6.8 Hz, indanimine H_5), 8.05 (2H, d, *J* = 8.3 Hz, methoxyphenyl CH), 11.28 (1H, brs, NH). ^{13}C-NMR (75 MHz, DMSO-d_6): δ = 27.8, 28.8, 55.7, 55.8, 102.4, 104.4, 114.3, 114.5, 118.5, 127.0, 127.6, 129.3, 139.2, 141.0, 148.7, 159.2, 159.5, 169.5. ESI-MS (*m*/*z*): $[M + H]^+$: 366.

2-(2-(6-methoxy-2,3-dihydro-1H-inden-1-ylidene)hydrazineyl)-4-(4-ciyanophenyl)thiazole (**2d**) Yield: 79%. M.P.: 262–264 °C. ^{1}H-NMR (300 MHz, DMSO-d_6): δ = 2.91 (2H, t, *J* = 7.1 Hz, –CH_2), 3.01 (2H, t, *J* = 6.9 Hz, –CH_2), 3.79 (3H, s, –OCH_3), 6.95 (1H, dd, *J* = 8.3 Hz, 2.5 Hz, indanimine H_4), 7.07 (1H, d, *J* = 2.4 Hz, indanimine H_2), 7.27 (1H, d, *J* = 8.3 Hz, indanimine H_5), 7.64 (1H, s, thiazole CH), 7.87 (2H, d, *J* = 8.5 Hz, cyanophenyl CH), 7.87 (2H, d, *J* = 8.5 Hz, cyanophenyl CH), 11.23 (1H, brs, NH). ^{13}C-NMR (75 MHz, DMSO-d_6): δ = 27.8, 28.8, 55.7, 104.2, 108.1, 109.9, 118.3, 119.5, 126.6, 126.9, 128.7, 133.2, 139.3, 140.7, 149.2, 157.0, 159.2, 170.2. ESI-MS (*m*/*z*): $[M + H]^+$: 361.

2-(2-(6-methoxy-2,3-dihydro-1H-inden-1-ylidene)hydrazineyl)-4-(4-nitrophenyl)thiazole (**2e**) Yield: 90%. M.P.: 242–244 °C. ^{1}H-NMR (300 MHz, DMSO-d_6): δ = 2.89 (2H, t, *J* = 6.3 Hz, –CH_2), 3.01 (2H, t, *J* = 6.1 Hz, –CH_2), 3.80 (3H, s, –OCH_3), 6.96 (1H, dd, *J* = 8.3 Hz, 2.5 Hz, indanimine H_4), 7.06 (1H, d, *J* = 2.4 Hz, indanimine H_2), 7.28 (1H, d, *J* = 8.3 Hz, indanimine H_5), 7.73 (1H, s, thiazole CH), 8.13 (2H, d, *J* = 9.0 Hz, nitrophenyl CH), 8.28 (2H, d, *J* = 9.0 Hz, nitrophenyl CH), 11.27 (1H, brs, NH). ^{13}C-NMR (75 MHz, DMSO-d_6): δ = 27.8, 28.7, 55.7, 104.2, 109.2, 118.3, 124.6, 126.8, 126.9, 139.3, 140.7, 141.3, 146.6, 149.0, 157.0, 159.2, 170.3. ESI-MS (*m*/*z*): $[M + H]^+$: 381.

2-(2-(6-methoxy-2,3-dihydro-1H-inden-1-ylidene)hydrazineyl)-4-(4-fluorophenyl)thiazole (**2f**) Yield: 87%. M.P.: 218–220 °C. ^{1}H-NMR (300 MHz, DMSO-d_6): δ = 2.87–2.91 (2H, m, –CH_2), 3.01 (2H, t, *J* = 6.9 Hz, –CH_2), 3.79 (3H, s, –OCH_3), 6.95 (1H, dd, *J* = 8.3 Hz, 2.5 Hz, indanimine H_4), 7.08 (1H, d, *J* = 2.5 Hz, indanimine H_2), 7.21–7.28 (4H, m, fluorophenyl CH, thiazole CH, indanimine H_5), 7.87–7.92 (2H, m, fluorophenyl CH), 11.31 (1H, brs, NH). ^{13}C-NMR (75 MHz, DMSO-d_6): δ = 27.8, 28.8, 55.7, 104.2, 115.6, 115.9 (d, J_{CF} = 21.3 Hz), 118.3, 126.9, 128.1 (d, J_{CF} = 8.1 Hz), 130.0, 130.9, 139.3, 140.7, 157.7, 159.2, 162.1 (d, J_{CF} = 243.0 Hz), 169.8. ESI-MS (*m*/*z*): $[M + H]^+$: 354.

2-(2-(6-methoxy-2,3-dihydro-1H-inden-1-ylidene)hydrazineyl)-4-(4-chlorophenyl)thiazole (**2g**) Yield: 84%. M.P.: 246–248 °C. ^{1}H-NMR (300 MHz, DMSO-d_6): δ = 2.89 (2H, t, *J* = 7.3 Hz, –CH_2), 3.00 (2H, t, *J* = 6.9 Hz, –CH_2), 3.80 (3H, s, –OCH_3), 6.95 (1H, dd, *J* = 8.3 Hz, 2.5 Hz, indanimine H_4), 7.07 (1H, d, *J* = 2.5 Hz, indanimine H_2), 7.27 (1H, d, *J* = 8.3 Hz, indanimine H_5), 7.39 (1H, s, thiazole CH), 7.47 (2H, d, *J* = 8.6 Hz, chlorophenyl CH), 7.88 (2H, d, *J* = 8.6 Hz, chlorophenyl CH), 11.23 (1H, brs, NH).

^{13}C-NMR (75 MHz, DMSO-d_6): δ = 27.8, 28.7, 55.7, 104.2, 118.3, 126.9, 127.7, 129.1, 130.0, 133.9, 139.3, 140.7, 149.3, 157.0, 159.2, 169.9. ESI-MS (*m*/*z*): $[M + H]^+$: 370.

2-(2-(6-methoxy-2,3-dihydro-1H-inden-1-ylidene)hydrazineyl)-4-(4-bromophenyl)thiazole (**2h**) Yield: 89%. M.P.: 224–226 °C. ^{1}H-NMR (300 MHz, DMSO-d_6): δ = 2.89 (2H, t, *J* = 5.9 Hz, –CH_2), 3.00 (2H, t, *J* = 6.0 Hz, -CH_2), 3.79 (3H, s, –OCH_3), 6.95 (1H, dd, *J* = 8.3 Hz, 2.5 Hz, indanimine H_4), 7.07 (1H, d, *J* = 2.4 Hz, indanimine H_2), 7.27 (1H, d, *J* = 8.3 Hz, indanimine H_5), 7.40 (1H, s, thiazole CH), 7.60 (2H, d, *J* = 8.6 Hz, bromophenyl CH), 7.81 (2H, d, *J* = 8.6 Hz, chlorophenyl CH), 11.17 (1H, brs, NH). ^{13}C-NMR (75 MHz, DMSO-d_6): δ = 27.8, 28.8, 55.7, 104.2, 105.2, 118.3, 121.0, 126.9, 128.1, 132.0, 134.1, 139.3, 140.7, 149.1, 157.2, 159.2, 169.9. ESI-MS (*m*/*z*): $[M + H]^+$: 414.

2-(2-(6-methoxy-2,3-dihydro-1H-inden-1-ylidene)hydrazineyl)-4-(2,4-dimethylphenyl)thiazole (**2i**) Yield: 85%. M.P.: 229–231 °C. ^{1}H-NMR (300 MHz, DMSO-d_6): δ = 2.31 (3H, s, –CH_3), 2.38 (3H, s, –CH_3), 2.91 (2H, t, *J* = 7.2 Hz, –CH_2), 3.03 (2H, t, *J* = 6.9 Hz, –CH_2), 3.79 (3H, s, –OCH_3), 6.93 (1H, s, thiazole CH), 6.99 (1H, dd, *J* = 8.3 Hz, 2.5 Hz, indanimine H_4), 7.08 (1H, d, *J* = 7.9 Hz, dimethylphenyl H_5), 7.12 (1H, brs, indanimine H_2), 7.17 (1H, brs, dimethylphenyl H_3), 7.30 (1H, d, *J* = 8.4 Hz, indanimine H_5), 7.45 (1H, d, *J* = 7.7 Hz, dimethylphenyl H_6) 11.56 (1H, brs, NH). ^{13}C-NMR (75 MHz, DMSO-d_6): δ = 21.1, 21.2, 27.9, 28.9, 55.8, 104.9, 106.6, 118.6, 126.9, 127.0, 130.0, 130.9, 131.8, 132.2, 136.1, 139.1, 141.2, 148.3, 159.2, 159.6, 168.4. ESI-MS (*m*/*z*): $[M + H]^+$: 364.

2-(2-(6-methoxy-2,3-dihydro-1H-inden-1-ylidene)hydrazineyl)-4-(2,4-dimethoxyphenyl)thiazole (**2j**) Yield: 86%. M.P.: 219–221 °C. ^{1}H-NMR (300 MHz, DMSO-d_6): δ = 2.91 (2H, t, *J* = 6.0 Hz, –CH_2), 3.02 (2H, t, *J* = 6.0 Hz, –CH_2), 3.80 (3H, s, –OCH_3), 3.81 (3H, s, –OCH_3), 3.90 (3H, s, –OCH_3), 6.62 (1H, dd, *J* = 8.6 Hz, 2.3 Hz, dimethoxyphenyl H_5), 6.67 (1H, d, *J* = 2.2 Hz, dimethoxyphenyl H_3), 6.98 (1H, dd, *J* = 8.3 Hz, 2.4 Hz, indanimine H_4), 7.11 (1H, brs, indanimine H_2), 7.21 (1H, s, thiazole CH), 7.29 (1H, d, *J* = 8.4 Hz, indanimine H_5), 7.90 (1H, d, *J* = 7.8 Hz, dimethylphenyl H_6), 11.28 (1H, brs, NH). ^{13}C-NMR (75 MHz, DMSO-d_6): δ = 27.8, 28.8, 55.8, 56.0, 56.1, 99.1, 104.4, 105.5, 105.7, 118.5, 127.0, 130.4, 133.8, 139.2, 140.9, 145.8, 148.1, 158.2, 158.9, 159.2, 167.9. ESI-MS (*m*/*z*): $[M + H]^+$: 396.

2-(2-(6-methoxy-2,3-dihydro-1H-inden-1-ylidene)hydrazineyl)-4-(2,4-difluorophenyl)thiazole (**2k**) Yield: 83%. M.P.: 200–202 °C. ^{1}H-NMR (300 MHz, DMSO-d_6): δ = 2.89 (2H, t, *J* = 6.3 Hz, –CH_2), 3.01 (2H, t, *J* = 6.2 Hz, –CH_2), 3.80 (3H, s, –OCH_3), 6.96 (1H, dd, *J* = 8.3 Hz, 2.6 Hz, indanimine H_4), 7.07 (1H, d, *J* = 2.4 Hz, indanimine H_2), 7.15–7.21 (2H, m, difluorophenyl CH, thiazole CH), 7.28 (1H, d, *J* = 8.3 Hz, indanimine H_5), 7.32–7.40 (1H, m, difluorophenyl CH), 8.02–8.11 (2H, m, difluorophenyl CH), 11.17 (1H, brs, NH). ^{13}C-NMR (75 MHz, DMSO-d_6): δ = 27.8, 28.7, 55.7, 104.1, 105.0 (t, *J* =26.2 Hz), 108.4 (d, *J* = 14.0 Hz), 112.3 (d, *J* = 21.1 Hz), 118.3, 119.5, 126.9, 130.8, 139.3, 140.7, 143.6, 156.9, 159.2, 159.2 (dd, *J* = 250.0 Hz, 12.1 Hz), 161.6 (dd, *J* = 246.1 Hz, 12.5 Hz), 169.3. ESI-MS (*m*/*z*): $[M + H]^+$: 372.

2-(2-(6-methoxy-2,3-dihydro-1H-inden-1-ylidene)hydrazineyl)-4-(2,4-dichlorophenyl)thiazole (**2l**) Yield: 88%. M.P.: 205–207 °C. ^{1}H-NMR (300 MHz, DMSO-d_6): δ = 2.88 (2H, t, *J* = 6.3 Hz, –CH_2), 3.01 (2H, t, *J* = 6.2 Hz, –CH_2), 3.79 (3H, s, –OCH_3), 6.96 (1H, dd, *J* = 8.3 Hz, 2.6 Hz, indanimine H_4), 7.07 (1H, d, *J* = 2.4 Hz, indanimine H_2), 7.28 (1H, d, *J* = 8.3 Hz, indanimine H_5), 7.40 (1H, s, thiazole CH), 7.51 (1H, dd, *J* = 8.6 Hz, 2.2 Hz, dichlorophenyl CH), 7.70 (1H, d, *J* = 2.2 Hz, dichlorophenyl CH), 7.93 (1H, d, *J* = 8.5 Hz, dichlorophenyl CH), 11.23 (1H, brs, NH). ^{13}C-NMR (75 MHz, DMSO-d_6): δ = 27.8, 28.7, 55.8, 104.2, 109.8, 118.3, 127.0, 128.0, 129.8, 130.2, 132.0, 132.7, 132.9, 139.3, 140.7, 146.2, 156.9, 159.2, 169.0. ESI-MS (*m*/*z*): $[M + H]^+$: 404.

3.2. Cholinesterase Enzymes Inhibition Assay

A cholinesterase enzyme inhibition assay was performed as in vitro using the modified Ellman's spectrophotometric method [15] to exhibit the AChE and BChE inhibition profiles of all the synthesized compounds (**2a**–**2l**). The enzymes (AChE (E.C.3.1.1.7, from *electric eel*) and BChE (from *equine serum*)), substrates (acetylthiocholine iodide (ATC) and butyrylthiocholine iodide (BTC)), chromogenic agent (5,5′-dithiobis-(2-nitrobenzoic acid) (DTNB)), and reference drugs (donepezil hydrochloride and tacrine) used in the enzyme inhibition procedure were all purchased commercially from Sigma-Aldrich

(Darmstadt, Germany) and Fluka (Buchs, Germany). The in vitro cholinesterase enzyme inhibition assay was applied as previously described by our research group [7,15–22].

The percentage of inhibition results and IC_{50} values, which were calculated using a dose-response curve achieved by plotting the percentage of inhibition versus the log concentration using the GraphPad PRISM software version 5.0 (San Diego, CA, USA), were shown as the mean ± standard deviation (SD).

3.3. Kinetic Studies of Enzyme Inhibition

The AChE enzyme kinetics study was performed for compound **2e** to determine the type of inhibition. Different concentrations (IC_{50}, 2 × IC_{50} and IC_{50}/2) of compound **2e** were prepared for this assay in addition to a substrate (ATC) at various concentrations (600, 300, 150, 75, 37.5, and 18.75 μM). The enzyme kinetics assay was carried out as in previous publications [7,16–22]. Lineweaver-Burk plots were formed using Microsoft Office Excel 2013. The K_i values of the compound were easily calculated from the second plot with a common intercept on the x-axis (corresponding to $-K_i$).

3.4. Inhibition of Beta Amyloid 1–42 (Aβ42) Aggregation

The test procedure was created based on the protocol of the beta amyloid 1–42 (Aβ42) ligand screening assay (BioVision, Milpitas, CA, USA), based on the fluorometric method.

3.5. Prediction of ADME Parameters and BBB Permeability

Physicochemical parameters were performed with the use of the *QikProp 4.8* software [23] to predict pharmacokinetic profiles and BBB permeability of obtained compounds (**2a**–**2l**).

3.6. Molecular Docking

A structure based in silico procedure was applied to discover the binding modes of compound **2e** to the *h*AChE enzyme active site. The crystal structures of *h*AChE (PDB ID: 4EY7) [12], which was crystallized with donepezil, was retrieved from the Protein Data Bank server (www.pdb.org).

The structures of ligands were built using the *Schrödinger Maestro* [40] interface and then were submitted to the *Protein Preparation Wizard* protocol of the *Schrödinger Suite 2016 Update 2* [41]. The ligands were prepared by the *LigPrep 3.8* [42] to assign the protonation states at pH 8.0 ± 1.0 and the atom types, correctly. Bond orders were assigned, and hydrogen atoms were added to the structures. The grid generation was formed using *Glide 7.1* [38]. Flexible docking runs were performed with a single precision docking mode (SP).

4. Conclusions

In conclusion, a new series of indan-thiazolylhydrazone derivatives was designed, and the inhibition profiles of the cholinesterase enzymes were evaluated. None of the synthesized compounds displayed remarkable enzyme activity on the BChE enzyme. All of the compounds showed selectivity against the AChE enzyme. Among the obtained compounds, derivatives of **2a**, **2e**, **2i**, and **2l** were found to be most active agents. Compound **2e**, which contained a 4-nitrophenyl ring, was determined to be the most effective inhibitor candidate, with an IC_{50} value of 0.026 μM. As a result of the docking studies, it was believed that the 6-methoxyindan moiety and 4-substituedphenyl-thiazole ring were essential for inhibiting the AChE enzyme. These structures were responsible for binding to the CAS and PAS regions of the enzyme active sites. Thus, it was observed that compound **2e** had a dual binding site feature by settling into the CAS and PAS, as did the donepezil molecule. Hence, all of the findings showed that the strategy of this study was correct and logical by structurally modifying the donepezil. These data provided the way to guide future studies.

Supplementary Materials: The following are available online at http://www.mdpi.com/2073-4352/10/8/637/s1. Table **S1**: IC_{50} values of compounds **2a**, **2e**, **2i**, **2l,** and donepezil against AChE. Figure **S1**: ^{1}H-NMR spectrum of compound **2a**. Figure **S2**: ^{13}C-NMR spectrum of compound **2a**. Figure **S3**: ^{1}H-NMR spectrum of compound **2b**. Figure **S4**: ^{13}C-NMR spectrum of compound **2b**. Figure **S5**: ^{1}H-NMR spectrum of compound **2c**. Figure **S6**: ^{13}C-NMR spectrum of compound **2c**. Figure **S7**: ^{1}H-NMR spectrum of compound **2d**. Figure **S8**: ^{13}C-NMR spectrum of compound **2d**. Figure **S9**: ^{1}H-NMR spectrum of compound **2e**. Figure **S10**: ^{13}C-NMR spectrum of compound **2e**. Figure **S11**: ^{1}H-NMR spectrum of compound **2f**. Figure **S12**: ^{13}C-NMR spectrum of compound **2f**. Figure **S13**: ^{1}H-NMR spectrum of compound **2g**. Figure **S14**: ^{13}C-NMR spectrum of compound **2g**. Figure **S15**: ^{1}H-NMR spectrum of compound **2h**. Figure **S16**: ^{13}C-NMR spectrum of compound **2h**. Figure **S17**: ^{1}H-NMR spectrum of compound **2i**. Figure **S18**: ^{13}C-NMR spectrum of compound **2i**. Figure **S19**: ^{1}H-NMR spectrum of compound **2j**. Figure **S20**: ^{13}C-NMR spectrum of compound **2j**. Figure **S21**: ^{1}H-NMR spectrum of compound **2k**. Figure **S22**: ^{13}C-NMR spectrum of compound **2k**. Figure **S23**: ^{1}H-NMR spectrum of compound **2l**. Figure **S24**: ^{13}C-NMR spectrum of compound **2l**.

Author Contributions: Y.Ö., A.S.K., and Z.A.K. conceived and designed the experiments; B.N.S. performed the synthesis, activity tests, and molecular docking studies; D.O., U.A.Ç., and B.K.Ç. performed the synthesis; D.O. and S.L. performed the analysis studies; B.N.S., D.O., U.A.Ç., S.L., B.K.Ç., Y.Ö., A.S.K., and Z.A.K. wrote the paper. All authors have read and agreed to the published version of the manuscript.

Funding: This study was financially supported by Anadolu University Scientific Projects Fund, Project No: 2005S055.

Conflicts of Interest: The authors declare no conflict of interest.

References

1. Sugimoto, H. The new approach in development of anti-Alzheimer's disease drugs via the cholinergic hypothesis. *Chem. Biol. Interact.* **2008**, *175*, 204–208. [CrossRef] [PubMed]
2. Costanzo, P.; Cariati, L.; Desiderio, D.; Sgammato, R.; Lamberti, A.; Arcone, R.; Salerno, R.; Nardi, M.; Masullo, M.; Oliverio, M. Design, Synthesis, and Evaluation of Donepezil-Like Compounds as AChE and BACE-1 Inhibitors. *ACS Med. Chem. Lett.* **2016**, *7*, 470–475. [CrossRef] [PubMed]
3. Cavdar, H.; Senturk, M.; Guney, M.; Durdagi, S.; Kayik, G.; Supuran, C.T.; Ekinci, D. Inhibition of acetylcholinesterase and butyrylcholinesterase with uracil derivatives: Kinetic and computational studies. *J. Enzym. Inhib. Med. Chem.* **2019**, *34*, 429–437. [CrossRef] [PubMed]
4. McHardy, S.F.; Wang, H.-Y.L.; McCowen, S.V.; Valdez, M.C. Recent advances in acetylcholinesterase Inhibitors and Reactivators: An update on the patent literature (2012–2015). *Expert Opin. Ther. Pat.* **2017**, *27*, 455–476. [CrossRef]
5. Rogers, S.L.; Friedhoff, L.T. Long-term efficacy and safety of donepezil in the treatment of Alzheimer's disease: An interim analysis of the results of a US multicentre open label extension study. *Eur. Neuropsychopharmacol.* **1998**, *8*, 67–75. [CrossRef]
6. Wang, Z.M.; Cai, P.; Liu, Q.H.; Xu, D.Q.; Yang, X.L.; Wu, J.J.; Kong, L.Y.; Wang, X.B. Rational modification of donepezil as multifunctional acetylcholinesterase inhibitors for the treatment of Alzheimer's disease. *Eur. J. Med. Chem.* **2016**, *123*, 282–297. [CrossRef]
7. Sağlık, B.N.; Ilgın, S.; Özkay, Y. Synthesis of new donepezil analogues and investigation of their effects on cholinesterase enzymes. *Eur. J. Med. Chem.* **2016**, *124*, 1026–1040. [CrossRef]
8. van Greunen, D.G.; Cordier, W.; Nell, M.; van der Westhuyzen, C.; Steenkamp, V.; Panayides, J.L.; Riley, D.L. Targeting Alzheimer's disease by investigating previously unexplored chemical space surrounding the cholinesterase inhibitor donepezil. *Eur. J. Med. Chem.* **2017**, *127*, 671–690. [CrossRef]
9. Youssef, K.M.; Fawzy, I.M.; El-Subbagh, H. N-substituted-piperidines as Novel Anti-alzheimer Agents: Synthesis, antioxidant activity, and molecular docking study. *Futur. J. Pharm. Sci.* **2018**, *4*, 1–7. [CrossRef]
10. Silva, D.; Chioua, M.; Samadi, A.; Agostinho, P.; Garção, P.; Lajarín-Cuesta, R.; Ríos, C.D.L.; Iriepa, I.; Moraleda, I.; González-Lafuente, L.; et al. Synthesis, Pharmacological Assessment, and Molecular Modeling of Acetylcholinesterase/Butyrylcholinesterase Inhibitors: Effect against Amyloid-β-Induced Neurotoxicity. *ACS Chem. Neurosci.* **2013**, *4*, 547–565. [CrossRef]
11. Lan, J.-S.; Zhang, T.; Liu, Y.; Yang, J.; Xie, S.-S.; Liu, J.; Miao, Z.-Y.; Ding, Y. Design, synthesis and biological activity of novel donepezil derivatives bearing N -benzyl pyridinium moiety as potent and dual binding site acetylcholinesterase inhibitors. *Eur. J. Med. Chem.* **2017**, *133*, 184–196. [CrossRef] [PubMed]

12. Cheung, J.; Rudolph, M.J.; Burshteyn, F.; Cassidy, M.S.; Gary, E.N.; Love, J.; Franklin, M.C.; Height, J.J. Structures of Human Acetylcholinesterase in Complex with Pharmacologically Important Ligands. *J. Med. Chem.* **2012**, *55*, 10282–10286. [CrossRef] [PubMed]
13. Huang, C.S.; Tu, W.T.; Luo, M.; Shi, J.G. Molecular Docking and Design of Novel Heterodimers of Donepezil and Huperzine Fragments as Acetylcholinesterase Inhibitors. *Chin. J. Struct. Chem.* **2016**, *35*, 839–848.
14. Vitorović-Todorović, M.D.; Worek, F.; Perdih, A.; Bauk, S.D.; Vujatovic, T.M.; Cvijetic, I.N. The in vitro protective effects of the three novel nanomolar reversible inhibitors of human cholinesterases against irreversible inhibition by organophosphorous chemical warfare agents. *Chem. Biol. Interact.* **2019**, *309*, 108714. [CrossRef]
15. Ellman, G.L.; Courtney, K.; Andres, V.; Featherstone, R.M. A new and rapid colorimetric determination of acetylcholinesterase activity. *Biochem. Pharmacol.* **1961**, *7*, 88–95. [CrossRef]
16. Özkay, Ü.D.; Can, Ö.D.; Sağlık, B.N.; Çevik, U.A.; Levent, S.; Özkay, Y.; Ilgin, S.; Atlı, Ö. Design, synthesis, and AChE inhibitory activity of new benzothiazole–piperazines. *Bioorg. Med. Chem. Lett.* **2016**, *26*, 5387–5394. [CrossRef]
17. Acar, Ç.U.; Levent, S.; Sağlık, B.N.; Özkay, Y.; Kaplancıklı, Z.A. Synthesis of Novel 4-(Dimethylaminoalkyl) piperazine-1-carbodithioa te Derivatives as Cholinesterase Inhibitors. *Lett. Drug Des. Discov.* **2017**, *14*, 528–539.
18. Levent, S.; Çevik, U.A.; Sağlık, B.N.; Özkay, Y.; Can, Ö.D.; Özkay, Ü.D.; Uçucu, Ü. Anticholinesterase activity screening of some novel dithiocarbamate derivatives including piperidine and piperazine moieties. *Phosphorus Sulfur Silicon Relat. Elem.* **2016**, *192*, 469–474. [CrossRef]
19. Hussein, W.; Sağlık, B.N.; Levent, S.; Korkut, B.; Ilgın, S.; Özkay, Y.; Kaplancıklı, Z.A. Synthesis and Biological Evaluation of New Cholinesterase Inhibitors for Alzheimer's Disease. *Molecules* **2018**, *23*, 2033. [CrossRef]
20. Tok, F.; Koçyiğit-Kaymakçıoğlu, B.; Sağlık, B.N.; Levent, S.; Özkay, Y.; Kaplancıklı, Z.A. Synthesis and biological evaluation of new pyrazolone Schiff bases as monoamine oxidase and cholinesterase inhibitors. *Bioorg. Chem.* **2019**, *84*, 41–50. [CrossRef]
21. Cevik, U.A.; Sağlık, B.N.; Levent, S.; Osmaniye, D.; Cavuşoglu, B.K.; Özkay, Y.; Kaplancikli, Z.A. Synthesis and AChE-Inhibitory Activity of New Benzimidazole Derivatives. *Molecules* **2019**, *24*, 861. [CrossRef] [PubMed]
22. Osmaniye, D.; Sağlık, B.N.; Çevik, U.A.; Levent, S.; Çavuşoğlu, B.K.; Özkay, Y.; Kaplancıklı, Z.A.; Turan, G. Synthesis and AChE Inhibitory Activity of Novel Thiazolylhydrazone Derivatives. *Molecules* **2019**, *24*, 2392. [CrossRef] [PubMed]
23. *QikProp, Version 4.8*; Schrödinger, LLC: New York, NY, USA, 2016.
24. Lipinski, C.A.; Franco, L.; Dominy Beryl, W.; Feeney Paul, J. Experimental and computational approaches to estimate solubility and permeability in drug discovery and development settings. *Adv. Drug Deliv. Rev.* **1997**, *23*, 3–25. [CrossRef]
25. Jorgensen, W.L.; Duffy, E.M. Prediction of drug solubility from structure. *Adv. Drug Deliv. Rev.* **2002**, *54*, 355–366. [CrossRef]
26. Daina, A.; Michielin, O.; Zoete, V. SwissADME: A free web tool to evaluate pharmacokinetics, drug-likeness and medicinal chemistry friendliness of small molecules. *Sci. Rep.* **2017**, *7*, 42717. [CrossRef] [PubMed]
27. Dunitz, J.D.; Taylor, R. Organic Fluorine Hardly Ever Accepts Hydrogen Bonds. *Chem. A Eur. J.* **1997**, *3*, 89–98. [CrossRef]
28. Dvir, H.; Silman, I.; Harel, M.; Rosenberry, T.L.; Sussman, J.L. Acetylcholinesterase: From 3D structure to function. *Chem. Interact.* **2010**, *187*, 10–22. [CrossRef]
29. Colovic, M.; Krstić, D.; Lazarevic-Pasti, T.; Bondžić, A.M.; Vasić, V.M. Acetylcholinesterase Inhibitors: Pharmacology and Toxicology. *Curr. Neuropharmacol.* **2013**, *11*, 315–335. [CrossRef]
30. Atanasova, M.; Stavrakov, G.; Philipova, I.; Zheleva-Dimitrova, D.; Yordanov, N.; Doytchinova, I. Galantamine derivatives with indole moiety: Docking, design, synthesis and acetylcholinesterase inhibitory activity. *Bioorg. Med. Chem.* **2015**, *23*, 5382–5389. [CrossRef]
31. Wu, M.-Y.; Esteban, G.; Brogi, S.; Shionoya, M.; Wang, L.; Campiani, G.; Unzeta, M.; Inokuchi, T.; Butini, S.; Marco-Contelles, J. Donepezil-like multifunctional agents: Design, synthesis, molecular modeling and biological evaluation. *Eur. J. Med. Chem.* **2016**, *121*, 864–879. [CrossRef]

32. Genest, D.; Rochais, C.; Lecoutey, C.; Jana Sopkova-de Oliveira, S.; Ballandonne, C.; Butt-Gueulle, S.; Legay, R.; Since, M.; Dallemagne, P. Design, synthesis and biological evaluation of novel indano-and thiaindano-pyrazoles with potential interest for Alzheimer's disease. *Med. Chem. Commun.* **2013**, *4*, 925–931. [CrossRef]
33. Al-Rashid, Z.F.; Hsung, R.P. A computational view on the significance of E-ring in binding of (+)-arisugacin A to acetylcholinesterase. *Bioorg. Med. Chem. Lett.* **2015**, *25*, 4848–4853. [CrossRef] [PubMed]
34. Alipour, M.; Khoobi, M.; Foroumadi, A.; Nadri, H.; Moradi, A.; Sakhteman, A.; Ghandi, M.; Shafiee, A. Novel coumarin derivatives bearing N-benzyl pyridinium moiety: Potent and dual binding site acetylcholinesterase inhibitors. *Bioorg. Med. Chem.* **2012**, *20*, 7214–7222. [CrossRef] [PubMed]
35. Cheung, J.; Gary, E.N.; Shiomi, K.; Rosenberry, T.L. Structures of Human Acetylcholinesterase Bound to Dihydrotanshinone I and Territrem B Show Peripheral Site Flexibility. *ACS Med. Chem. Lett.* **2013**, *4*, 1091–1096. [CrossRef] [PubMed]
36. Lee, Y.-H.; Yu, L.; Wang, H.; Fang, W.; Ling, X.; Shi, Y.; Lin, C.-T.; Huang, J.-K.; Chang, M.-T.; Chang, C.-S.; et al. Synthesis and Transfer of Single-Layer Transition Metal Disulfides on Diverse Surfaces. *Nano Lett.* **2013**, *13*, 1852–1857. [CrossRef]
37. Vitorović-Todorović, M.D.; Koukoulitsa, C.; Juranic, I.O.; Mandic, L.; Drakulić, B.J. Structural modifications of 4-aryl-4-oxo-2-aminylbutanamides and their acetyl- and butyrylcholinesterase inhibitory activity. Investigation of AChE–ligand interactions by docking calculations and molecular dynamics simulations. *Eur. J. Med. Chem.* **2014**, *81*, 158–175. [CrossRef]
38. *Glide, Version 7.1*; Schrödinger, LLC: New York, NY, USA, 2016.
39. Finkielsztein, L.M.; Castro, E.F.; Fabián, L.E.; Moltrasio, G.Y.; Campos, R.H.; Cavallaro, L.V.; Moglioni, A.G. New 1-indanone thiosemicarbazone derivatives active against BVDV. *Eur. J. Med. Chem.* **2008**, *43*, 1767–1773. [CrossRef] [PubMed]
40. *Maestro, Version 10.6*; Schrödinger, LLC: New York, NY, USA, 2016.
41. Available online: https://www.schrodinger.com/ (accessed on 20 May 2020).
42. *LigPrep, Version 3.8*; Schrödinger, LLC: New York, NY, USA, 2016.

Sample Availability: Samples of the compounds **2a-2l** are available from the authors.